



Research Paper

Design and optimisation of bump-enhanced conditioning rollers for uniform alfalfa stem damage

Qiao Jin ^a, Hongqian Li ^b, Decheng Wang ^{a,*}, Yong You ^a, Yunting Hui ^a, Sibiao Li ^a ^a College of Engineering, China Agricultural University, Beijing, 100083, China^b Shandong Wuzheng Group Co., Ltd, Shandong, 262399, China

ARTICLE INFO

Keywords:

Conditioning model
Surface structure design
Response surface test

ABSTRACT

Conditioning is a critical step in alfalfa hay harvesting, directly influencing its quality. A conditioning model was developed to identify the key factors affecting conditioning effectiveness. To address the issue of uneven stem damage caused by conventional conditioning rollers, a surface bump structure was designed. By arranging these bumps spatially, the rollers applied micro-rubbing actions to the alfalfa stems, thereby enhancing structural disruption. Parametric optimisation studies clarified how bump diameter, non-interference distance and helix angle influence stem disruption efficiency. The design was further refined using the finite element method. Subsequently, a Box-Behnken experimental design was employed to optimise three key operational parameters: feed rate, roller gap, and roller rotational speed. Drying tests were then conducted to compare the conditioning performance of different roller designs. Results showed that the minimum number of broken branches (0.67) and maximum number of non-fracture damage occurrences (7.67) were achieved with a bump diameter of 2.85 mm, a non-interference distance of 1.61 mm, and a helix angle of 23.85°. Aiming to maximise the conditioning while minimising the conditioning loss rate and energy consumption, the optimal parameters were determined to be a roller rotational speed of 683 r min⁻¹, a roller gap of 3.13 mm and a feed rate of 779 g s⁻¹. The moisture content of alfalfa conditioned using the roller with bumps dropped to around 40 % within the first 60 min. Compared with the other two conditioning rollers, this design demonstrated superior performance.

Nomenclature

Abbreviations

HTCR	Hexagonal-toothed conditioning roller
RTCH	Rectangular-toothed conditioning roller
Symbols	
A	Bump diameter (mm)
a	Side length of the rhombus (mm)
a _{min}	Minimum side length at which no interference occurs between bumps (mm)
B	Non-interference distance (mm)
B _r	Conditioning loss rate (%)
C	Helix angle of conditioning roller (°)
C _r	Conditioning rate (%)
D	Roller gap (mm)
E	Feed rate (g s ⁻¹)
F _{G(t)}	Normal pressure (N)
F _{Gx(t)}	Lateral component of the infinitesimal resultant force at time t (N)
F _{Gy(t)}	Vertical component of the infinitesimal resultant force at time t (N)
F _m	Intermediate variable

(continued on next column)

(continued)

F _{Tx}	Component of the force exerted by the bump on the alfalfa stem along the x-axis (N)
F _{Ty}	Component of the force exerted by the bump on the alfalfa stem along the y-axis (N)
F _{Tz}	Component of the force exerted by the bump on the alfalfa stem along the z-axis (N)
f _{Tm}	Frictional force exerted by the m-th bump (N)
h _c	Height of the rolling teeth (mm)
h _j	Minimum roller gap (mm)
i, j, k	Selected axes (x-axis, y-axis, z-axis) in the computational directions
L _g	Alfalfa thickness (mm)
L _m	Normal pressure (N)
m	Total mass of alfalfa (kg)
m _b	Mass of alfalfa lost or broken into small pieces (kg)
m _c	Mass of alfalfa meeting the conditioning criteria (kg)
m _d	Dry mass of alfalfa (kg)
m _f	Fresh mass of alfalfa (kg)
m _{ft}	Mass of alfalfa at time t (kg)
N	Roller rotational speed (r min ⁻¹)

(continued on next page)

* Corresponding author.

E-mail address: wdc@cau.edu.cn (D. Wang).

(continued)

N_1	Normal force exerted by the roller teeth on the alfalfa (N)
N_2	Normal force exerted by the tooth groove on the alfalfa (N)
N_b	Average number of broken branches
N_c	Average number of non-fracture damage occurrences
N_{Tm}	Normal force exerted by the m -th bump on the stem (N)
n_c	Number of roller teeth in contact with the alfalfa
R_1	Radius of the tooth tip circle (mm)
R_2	Radius of the tooth root circle (mm)
r	Radius of the bump (mm)
$S_t(t)$	Contact area between the roller teeth and the material at time t (mm^2)
s	Width of the roller teeth (mm)
$s_g(t)$	Lateral displacement from the contact point to minimum roller gap (mm)
T_0	No-load torque of the test bench (N m)
$T(t)$	Torque at time t (N m)
t	Time (s)
W_0	No-load energy of the test bench (J)
W_1	Total energy consumed during the conditioning process (J)
W_f	Moisture content of alfalfa (%)
W_{FS}	Conditioning energy required for the conditioning process (J kg^{-1})
W_{gx}	Work done by the lateral force of a single roller tooth (J)
W_{gy}	Work done by the vertical force of a single roller tooth (J)
W_{TS}	Conditioning energy (J kg^{-1})
Greek symbols	
β	Helix angle (rad)
η_e	Conditioning energy error (%)
θ_d	Friction angle between the alfalfa and the lower conditioning roller (rad)
θ_u	Friction angle between the alfalfa and the upper conditioning roller (rad)
μ_1	Coefficient of friction between the alfalfa and the roller teeth
μ_2	Coefficient of friction between the alfalfa and the tooth groove
ω	Angular velocity (rad s^{-1})

1. Introduction

The development of animal husbandry has diversified human dietary choices. However, greenhouse gases such as methane and nitrous oxide emitted by livestock, along with other pollutants, place a considerable burden on the environment (Razzaghi et al., 2022). In response to these challenges, high-quality protein feed has become essential for sustainable animal husbandry (Bacenetti et al., 2018; Hualing, Yanping, Yu, & Tai, 2021; Wang & Zou, 2020). Alfalfa, a perennial legume plant with strong adaptability, contributes to soil improvement through nitrogen fixation by its roots (Iannucci et al., 2002; Zhang et al., 2023). Due to the variation in its nutritional composition at different growth stages, alfalfa offers great flexibility as animal feed (Palmonari et al., 2014). Notably, from the early stage of budding to the early stage of flowering, alfalfa is rich in protein and is widely recognised as a commercial dairy feed in many countries (Kulkarni et al., 2018; Neres et al., 2010; Suwignyo et al., 2023). Studies have shown that cows fed with alfalfa exhibit significantly increased milk yield and milk protein content (Chowdhury

et al., 2023; Zhang et al., 2023). Alfalfa harvesting methods are categorised into silage and hay production, mainly differentiated by harvest timing and moisture content. As illustrated in Fig. 1, silage alfalfa is typically harvested at the early budding stage, while alfalfa for hay is usually harvested from budding to early flowering (Wang et al., 2017). A moisture content of 40 %–50 % serves as the threshold between silage and hay. Silage alfalfa requires a moisture content above 40 % to prevent mould growth caused by overheating. In contrast, alfalfa below this range must be further dried to under 20 % moisture content before being baled as hay (Wang et al., 2017). Alfalfa leaves and stems evaporate water at different rates, and excessive drying rate differentials and prolonged drying times can lead to leaf shedding and reduced feed quality—particularly during hay production (Bacenetti et al., 2018; Galyon et al., 2024). Related studies have shown that there is a 22 % loss of leaves during the hay-making process (Rade et al., 2019). To mitigate this, it is necessary to mechanically disrupt the surface fibres of alfalfa stems during harvesting. Conditioners, the main mechanisms for this purpose, are classified into impeller and roller types (Fig. 2). While impeller conditioners inflict more severe damage to stems, they also cause greater nutrient loss compared to roller conditioners (Greenlees et al., 2000). Roller conditioners work by squeezing and bending alfalfa stems between two counter-rotating rollers to rupture surface fibres. Greenlees et al. (2000) compared the drying rates and leaf loss in alfalfa using three impeller conditioners and one roller conditioner. They found that rotational speed significantly influenced both metrics. The drying rate using a high-speed impeller conditioner was 23–63 % higher than that achieved with a high-speed roller conditioner, but with 1.7–3.4 % more leaf loss. Fychan et al. (2016) studied protein loss in forage under three conditions: no conditioning, steel roller conditioning and rubber roller conditioning. Although steel roller conditioning produced slightly higher silage dry matter, it significantly reduced nitrogen content. Shinners et al. (2006) examined how roller type, roller gap, and feed rate influenced drying rate and leaf loss in alfalfa. They observed that steel rollers had a larger crushing area than polyurethane rollers, resulting in a 7 % increase in drying rate post-conditioning. Song et al. (2021) developed a measurement and control system for an alfalfa conditioning test bench, analysing energy consumption per unit, conditioning rate and conditioning loss rate under operational conditions. Suwarno et al. (1999) investigated the changes in microbial communities and nutrient profiles in alfalfa after conditioning. Jin et al. (2024) conducted parameter calibration and experimental validation for a finite element model of alfalfa conditioning, identifying optimal stem material parameters. Qiao et al. (2024) designed a hexagonal-toothed conditioning roller (HTCR), which effectively reduced stem breakage losses during the conditioning compared with the traditional rectangular-toothed roller (RTCH).

The core challenge in alfalfa conditioning technology lies in

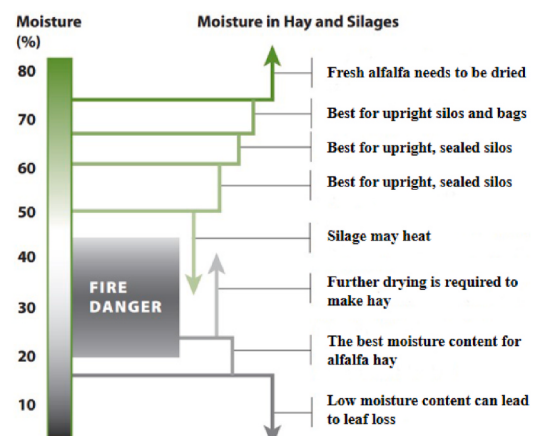
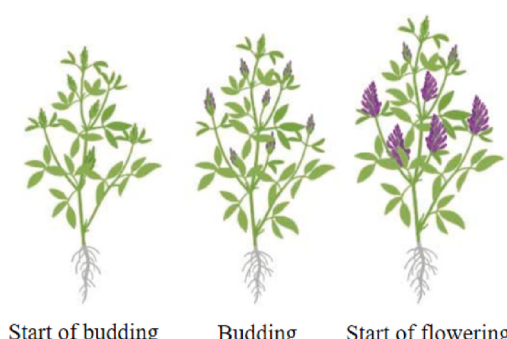


Fig. 1. Harvesting period and moisture content requirements for alfalfa hay and silage feed.

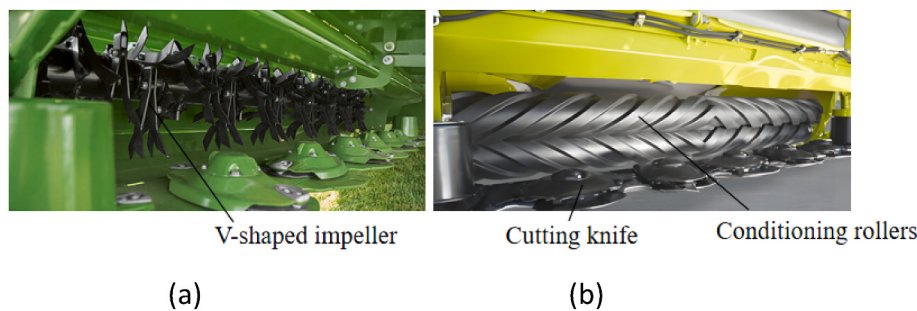


Fig. 2. Impeller and roller conditioners. (a) impeller conditioner (KRONE 450) and (b) roller conditioner (CLASS 3050).

effectively disrupting stem fibres while minimising mechanical losses (Bacenetti et al., 2018; Jin et al., 2024). Previous studies have gradually enhanced drying efficiency through comparisons between impeller-type and roller-type conditioners (Greenlees et al., 2000), optimisation of roller parameters (Shinnars et al., 2006), and the development of novel roller tooth structures (Jin et al., 2024). However, systematic reviews highlight two persistent limitations in current conditioning processes: first, traditional rollers often result in uneven stem disruption following conditioning (Jin et al., 2024); second, the trade-off between achieving a higher drying rate and minimising mechanical losses has yet to be resolved through structural innovations (Fychan et al., 2016). To address these issues, this study proposes a hemispherical-bump roller design. The bump geometry and key operational parameters of the conditioning rollers are optimised using finite element method (FEM) simulations in conjunction with response surface methodology (RSM), with the objective of achieving more uniform fibre disruption in alfalfa stems.

2. Materials and methods

2.1. Stress analysis during the conditioning process

The conditioning roller consists of a steel core and an outer profile, typically made from rubber or thermoplastic polyurethane (TPU). During the conditioning process, the roller teeth and grooves intermesh to compress and bend the alfalfa stems. Given that the height of the roller teeth is not negligible in relation to the stem diameter, the compression mechanism can be simplified as the interaction between two rollers of differing radii rotating at the same speed, as illustrated in Fig. 3 (Jin et al., 2024). By selecting an arbitrary position during the conditioning process, the force acting on the alfalfa can be described using Eq. (1) (Jin et al., 2024):

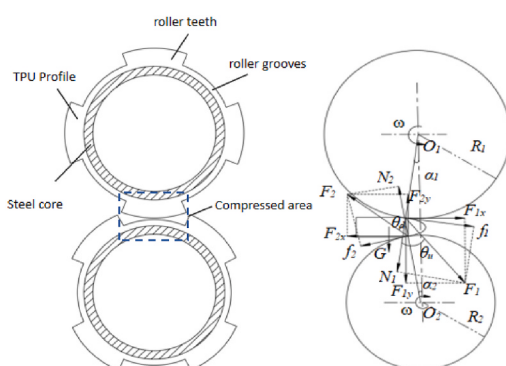


Fig. 3. Schematic diagram of the stress on alfalfa during the conditioning process.

$$\begin{cases} f_1 = \mu_1 N_1 = N_1 \tan \theta_u \\ f_2 = \mu_2 N_2 = N_2 \tan \theta_d \\ F_1 = N_1 \cos \theta_u \\ F_2 = N_2 \cos \theta_d \end{cases} \quad (1)$$

where N_1 is the normal force exerted by the roller teeth on the alfalfa (N); N_2 is the normal force exerted by the tooth groove on the alfalfa (N); f_1 is the frictional force from the roller teeth acting on the alfalfa (N); f_2 is the frictional force from the groove acting on the alfalfa (N); μ_1 is the coefficient of friction between the alfalfa and the upper conditioning roller (rad); μ_2 is the coefficient of friction between the alfalfa and the lower conditioning roller (rad); F_1 is the net force exerted by the roller teeth on the alfalfa (N); and F_2 is the net force exerted by the tooth groove on the alfalfa (N).

By decomposing the forces F_1 and F_2 into their horizontal and vertical components and substituting them into Eq. (1), Eq. (2) can be obtained:

$$\begin{cases} F_{1x} = f_1 \cos \alpha_1 - N_1 \sin \alpha_1 = N_1(\mu_1 \cos \alpha_1 - \sin \alpha_1) \\ F_{2x} = f_2 \cos \alpha_2 + N_2 \sin \alpha_2 = N_2(\mu_2 \cos \alpha_2 + \sin \alpha_2) \\ F_{1y} = F_{1x} \tan(\theta_u - \alpha_1) \\ F_{2y} = F_{2x} \tan(\theta_d - \alpha_2) \end{cases} \quad (2)$$

where α_1 and α_2 are the angles between the line connecting the contact point to the centre of the respective roller and the line connecting the centres of the upper and lower rollers (rad); F_{1x} and F_{2x} are the horizontal components of the resultant forces F_1 and F_2 , respectively (N); and F_{1y} and F_{2y} are the vertical components of the resultant forces F_1 and F_2 , respectively (N).

2.2. Alfalfa conditioning model

To identify the primary factors influencing the conditioning effect, a conditioning model was established. Prior to model development, appropriate simplifications of the boundary conditions were made. It is assumed that, during conditioning, the alfalfa forms a continuous material flow with a thickness of L_g , and the grass strips exhibit symmetry along the x -axis, as illustrated in Fig. 4. The centre line O_1O_2 intersects the upper and lower rollers at points B_{g1} and B_{g2} , respectively. It is further assumed that the material contacts the roller teeth and grooves at points A_{g1} and A_{g2} , respectively. As the upper and lower rollers rotate, the alfalfa is progressively compressed in the y -direction. When A_{g1} coincides with B_{g1} , and A_{g2} with B_{g2} , the material reaches its maximum compression stage, corresponding to the minimum roller gap. Based on the geometric relationships shown in Fig. 4, Eq. (3) is derived:

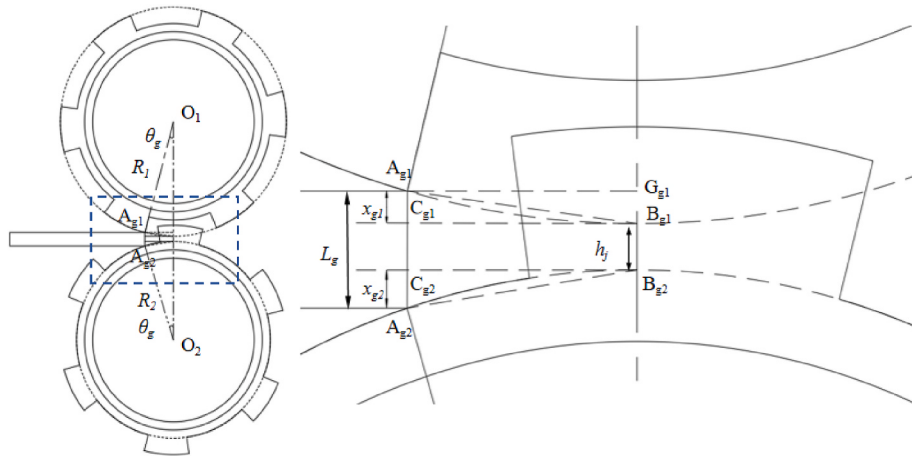


Fig. 4. Schematic diagram of alfalfa deformation during conditioning process.

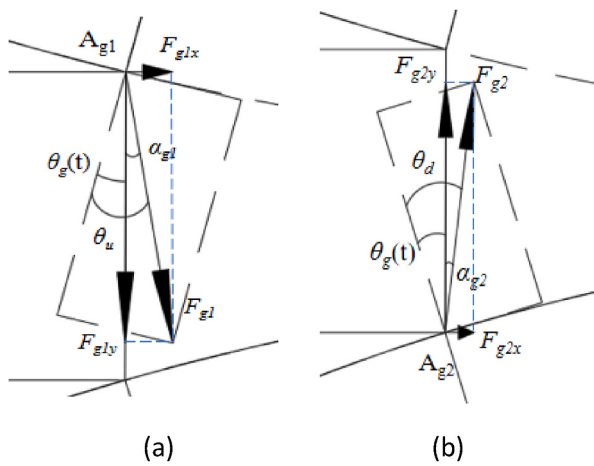


Fig. 5. Force analysis at the contact points between alfalfa and the conditioning roller: (a) contact point between roller teeth and alfalfa and (b) contact point between the tooth groove and alfalfa.

$$\begin{cases} x_{g1} = \frac{L_g - h_j}{1 + \frac{R_2}{R_1}} \\ x_{g2} = (L_g - h_j) \left(1 - \frac{1}{1 + \frac{R_2}{R_1}} \right) \\ R_d = \frac{R_2}{1 + \frac{R_1}{R_2}} \\ \theta_g = \arccos \frac{R_1 - x_{g1}}{R_1} = \arccos \frac{R_1 - x_{g2}}{R_1} \end{cases} \quad (3)$$

where L_g is the alfalfa thickness (mm); x_{g1} and x_{g2} are the displacements of the material in the y -direction during compression (mm); θ_g is the angle between O_1O_2 and O_1A_{g1} (rad); h_j is the minimum roller gap (mm); R_1 is the radius of the tooth tip circle (mm); and R_2 is the radius of the tooth root circle (mm).

According to the work-energy theorem, the work performed by a single roller tooth on the alfalfa can be analysed by examining the infinitesimal contact region between the alfalfa and the roller teeth. As

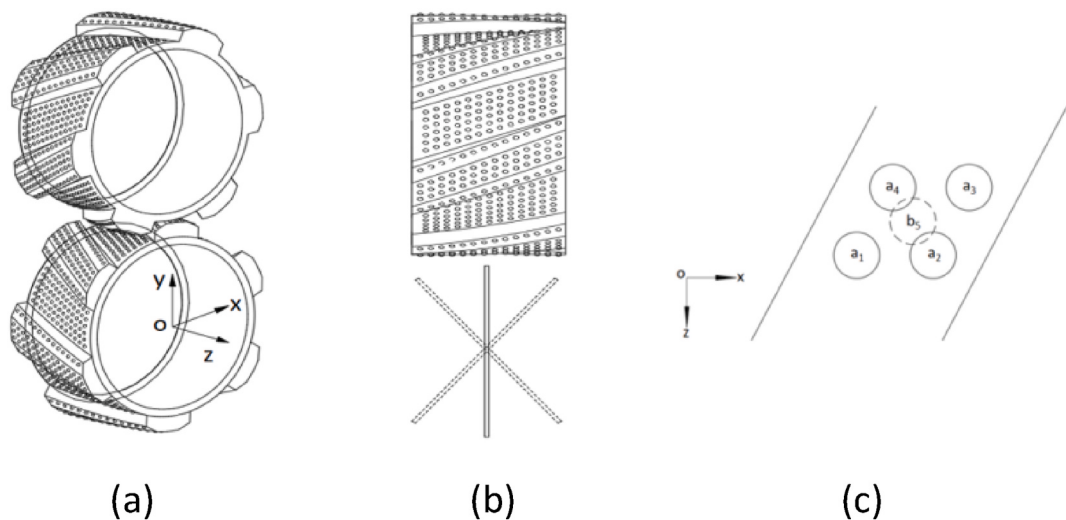


Fig. 6. Schematic diagram of HTCR (with bumps): (a) Cartesian coordinate system, (b) vertical view of conditioning roller and (c) projection of bumps on the xoz plane.

previously discussed, the work is done from the moment the alfalfa first contacts the roller tooth until the roller gap reaches its minimum value. The force distribution at the contact point is illustrated in Fig. 5. By decomposing the resultant force into horizontal and vertical components, Eqs (4)–(6) are derived.

$$\begin{cases} F_{g1} = \frac{F_{g1y}}{\cos \alpha_{g1}} \\ F_{g1x} = F_{g1y} \tan \alpha_{g1} \\ \alpha_{g1} = \theta_u - \theta_g(t) \end{cases} \quad (4)$$

$$\begin{cases} F_{g2} = \frac{F_{g2y}}{\cos \alpha_{g2}} \\ F_{g2x} = F_{g2y} \tan \alpha_{g2} \\ \alpha_{g2} = \theta_d - \theta_g(t) \end{cases} \quad (5)$$

$$\theta_g(t) = \omega \cdot t \quad (6)$$

where $\theta_g(t)$ is the angle between the line O_1O_2 and O_1A_{g1} at time t (rad); and ω is the angular velocity of the roller (rad s⁻¹).

The friction angle between the roller teeth and the alfalfa is generally assumed to be equal to that between the tooth groove and the alfalfa, such that $\theta_d = \theta_u$. To simplify the calculations, the following assumptions are made: (1) Because the thickness of alfalfa is less than the roller diameter, it is assumed that $x_{g2} = x_{g1}$. (2) The effect of gravitational force at the contact point is neglected, resulting in $F_{g1y} = F_{g2y} = F_{gy}$ and $\alpha_{g1} = \alpha_{g2}$. (3) The uneven distribution of stress caused by factors such as alfalfa geometry and roller tooth deformation is disregarded. It is also assumed that the horizontal velocity component of the alfalfa remains constant as it enters the gap between the upper and lower rollers. The conditioning roller, characterised by a helix angle β , leaves an indentation of length P_g on the alfalfa, with a contact width of C_g . By combining Eqs (3)–(6), the conditioning energy expressions for a single roller tooth can be derived, as shown in Eqs (7)–(9).

$$\begin{cases} W_{gx} = \int_0^s \int_0^{P_g} W_{g1x} dx dy + \int_0^s \int_0^{P_g} W_{g2x} dx dy \\ W_{g1x} = \int_{t_1}^{t_2} F_{gx}(t) s_{g1}(t) dt \\ W_{g2x} = \int_{t_1}^{t_2} F_{gx}(t) s_{g2}(t) dt \\ F_{gx}(t) = F_{gy}(t) \tan(\theta_u - \omega t) \\ s_{g1}(t) \approx s_{g2}(t) = s_g(t) = \frac{\omega \cdot R_1 \sin \theta_g}{\theta_g} t \end{cases} \quad (8)$$

$$\begin{cases} F_{gy}(t) = \begin{cases} \frac{F_G(t)}{\frac{1}{2} s_g(t) \tan \beta} & 0 \leq s_g(t) \leq C_g \cdot \tan \beta \\ \frac{F_G(t)}{\frac{1}{2} C_g^2 \tan \beta + (s_g(t) - C_g \tan \beta) C_g} & C_g \cdot \tan \beta \leq s_g(t) \leq s \\ \frac{F_G(t)}{F_m} & s \leq s_g(t) \leq s + C_g \cdot \tan \beta \end{cases} \\ F_m = (s - C_g \tan \beta) C_g + C_g^2 \tan \beta - \frac{1}{2} (s + 2C_g \tan \beta - s_g(t))^2 \tan \beta \end{cases} \quad (9)$$

where W_{gx} is the work done by the lateral force of a single roller tooth (J); W_{gy} is the work done by the vertical force of a single roller tooth (J); $F_{gy}(t)$ is the vertical component of the infinitesimal resultant force at time t (N); $F_{gx}(t)$ is the lateral component of the infinitesimal resultant force at time t (N); $F_G(t)$ is the normal pressure during the conditioning process, which can be measured using sensors (N); s is the width of the roller teeth (mm); $S_t(t)$ is the contact area between the roller teeth and the material at time t (mm²); F_m is an intermediate variable; and $s_g(t)$ is the lateral displacement from the contact point to minimum roller gap (mm).

$$\begin{cases} W_{FS} = \frac{n_c}{m} \left(2 \int_0^s \int_0^{\frac{C_g}{\cos \beta}} \int_{t_1}^{t_2} F_{gy}(t) x_g(t) dt dx dy + 2 \int_0^s \int_0^{\frac{C_g}{\cos \beta}} \int_{t_1}^{t_2} F_{gx}(t) s_g(t) dt dx dy \right) \\ n_c = \frac{L_m}{\frac{s}{\cos \beta} + h_c} \end{cases} \quad (10)$$

$$\begin{cases} W_{gy} = \int_0^s \int_0^{P_g} W_{g1y} dx dy + \int_0^s \int_0^{P_g} W_{g2y} dx dy \\ W_{g1y} = \int_{t_1}^{t_2} F_{gy}(t) x_{g1}(t) dt \\ W_{g2y} = \int_{t_1}^{t_2} F_{gy}(t) x_{g2}(t) dt \\ F_{gy}(t) = \frac{dF_G(t)}{dS_t(t)} \\ P_g = \frac{C_g}{\cos \beta} \\ x_{g1}(t) \approx x_{g2}(t) = \frac{(L_g - h_j)}{2\theta_g} \omega t \end{cases} \quad (7)$$

where W_{FS} is the conditioning energy required for the conditioning process (J kg⁻¹); n_c is the number of roller teeth in contact with the alfalfa; L_m is the total length of the alfalfa (mm); h_c is the height of the roller teeth (mm); and m is the total mass of alfalfa (kg).

According to Eq. (10), the factors influencing the conditioning effect are categorised into operational parameters and structural parameters. The operational parameters include roller gap, alfalfa feed rate and roller rotational speed. The structural parameters comprise the friction coefficient between the alfalfa and conditioning rollers, the helix angle of the roller teeth, and the number and shape of the roller teeth.

2.3. Design of surface bumps on the conditioning roller

To effectively disrupt the fibres of alfalfa stems during conditioning, this study designed a conditioning roller featuring crossed hemispherical bumps. These hemispherical bumps have smooth surfaces without edges and corners, enabling more uniform compression and rubbing of

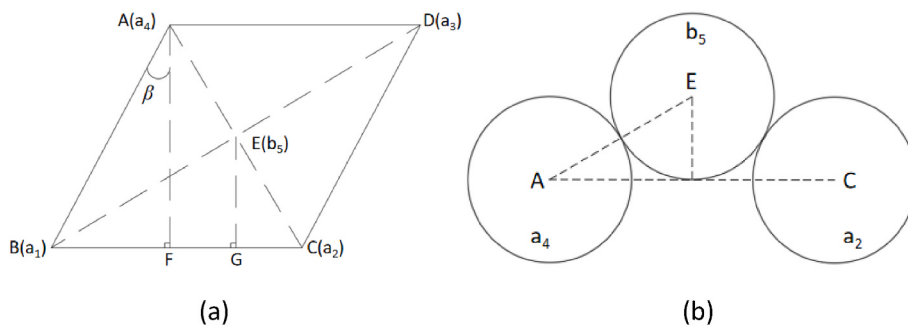


Fig. 7. Schematic diagram of convex point projections on the xoz and AEC planes: (a) projection on the xoz plane and (b) projection on the AEC plane.

the alfalfa stems. Even when the gap between the rollers is small, some space remains, which helps reduce damage to the leaves and lateral branches. A spatial Cartesian coordinate system was established with the origin at the centre of the cross-section of the conditioning roller, where the oz -axis is aligned parallel to the roller's axis, as illustrated in Fig. 6(a). During harvesting, the cut alfalfa enters the gap between the two conditioning rollers in random orientations due to airflow, as shown in Fig. 6(b). To achieve even fibre disruption, the projections of four adjacent bumps onto the xoz plane were arranged in a diamond pattern. During the conditioning process, stem compression is achieved through the matching of teeth from one roller with the grooves of the opposing roller. Consequently, the four adjacent bumps on one roller and a corresponding bump on the other roller constitute a minimum unit set, as depicted in Fig. 6(c). Additional bumps are generated by applying rotational and translational symmetry to this fundamental set.

The arrangement of the five bumps (A–E) on the xoz plane and the plane AEC is illustrated in Fig. 7(a). According to the geometric relationships shown in Fig. 7(a), the diagonal AC (L_{AC}) satisfies Eq. (11).

$$L_{AC} = (a \cos \beta)^2 + (a - a \sin \beta)^2 = 2a^2(1 - \sin \beta) \quad (11)$$

where a is the side length of the rhombus (mm).

Plane AEC passes through edge ac and is perpendicular to the xoz plane, as shown in Fig. 7(b). To ensure that the bumps do not interfere with each other when the gap of the conditioning roller varies from zero, the diagonal L_{AC} must satisfy Eq. (12).

$$L_{AC} \geq 4r \cos \frac{\pi}{6} \quad (12)$$

where r is the radius of the bump (mm).

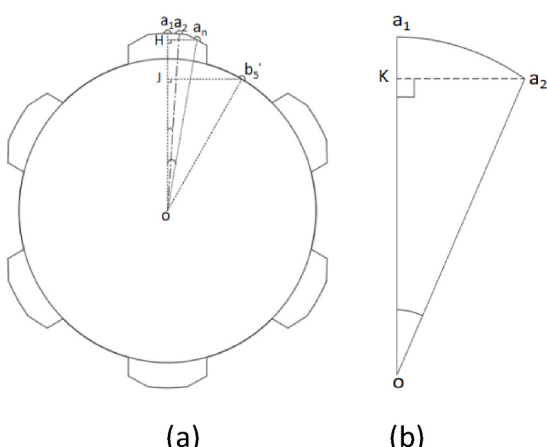


Fig. 8. Schematic diagram of bump projections on the xoy plane: (a) overall view and (b) partial view.

By combining Eqs (11) and (12), the side length a satisfies Eq. (13).

$$a \geq a_{\min} = \sqrt{\frac{L_{AC(\min)}^2}{2(1 - \sin \beta)}} \quad (13)$$

where a_{\min} is the minimum side length at which no interference occurs between bumps (mm).

Because EG is perpendicular to edge BC , triangles $\triangle EGC$ and $\triangle BEC$ are similar. Assuming the coordinates of point B are $(0, 0, z_1)$, the coordinates of the other points, according to the geometric relationships shown in Fig. 8(a) and (b), are as follows: $A(a \sin \beta, 0, z_1 - a \cos \beta)$, $C(a, 0, z_1)$, $D(a + a \sin \beta, 0, z_1 - a \cos \beta)$, $E(a - a^3(1 - \sin \beta)^2, 0, z_1 - a^2(1 - \sin \beta)\sin[\arccos(a - a \sin \beta)])$.

Fig. 8 is a schematic diagram showing the projection of the conditioning roller onto the xoy plane. A perpendicular line is drawn from point a_2 to oa_1 , with the foot of the perpendicular denoted as K . Based on this projection, the length of a_2K is a , and the corresponding central angle is given by Eq. (14).

$$\angle a_1 o a_2 = \arcsin \frac{a}{R_1} \quad (14)$$

Eq. (15) is derived from the geometric relationships illustrated in Fig. 8.

$$a_1 K = R_1 - R_1 \cos \left(\arcsin \frac{a}{R_1} \right) \quad (15)$$

Replace bump b_5 with bump b_5' , and group all bumps on the same conditioning roller for coordinate transformation. The central angles of bump b_5' and b_5 differ by 60° . From the intersection point b_5' , draw a perpendicular line to a_1o , denoted as J . Based on the coordinates of point E on the projection plane xoz and the geometric relationship shown in Fig. 8, Eqs (16) and (17) are derived.

$$b_5' J = R_2 \sin \left(\frac{\pi}{3} + \arcsin \frac{a - a^3(1 - \sin \beta)^2}{R_1} \right) \quad (16)$$

$$oJ = R_2 \cos \left(\frac{\pi}{3} + \arcsin \frac{a - a^3(1 - \sin \beta)^2}{R_1} \right) \quad (17)$$

Due to the obtuse-angled teeth of the HTCR effectively damaging stem fibres, no bumps were added at the edges. Starting from bump a_1 , when bump a_n lies on the inclined surface of the roller teeth, a perpendicular line a_1o is drawn through point a_n , with the foot of the perpendicular denoted as H . According to the projection relationship, $a_nH = na$ and $\angle a_noH = n\angle a_1o a_2$. Based on the geometric relationships shown in Fig. 8, Eq. (18) is derived.

$$oH = \frac{na}{\tan \left(n \arcsin \frac{a}{R_1} \right)} \quad (18)$$

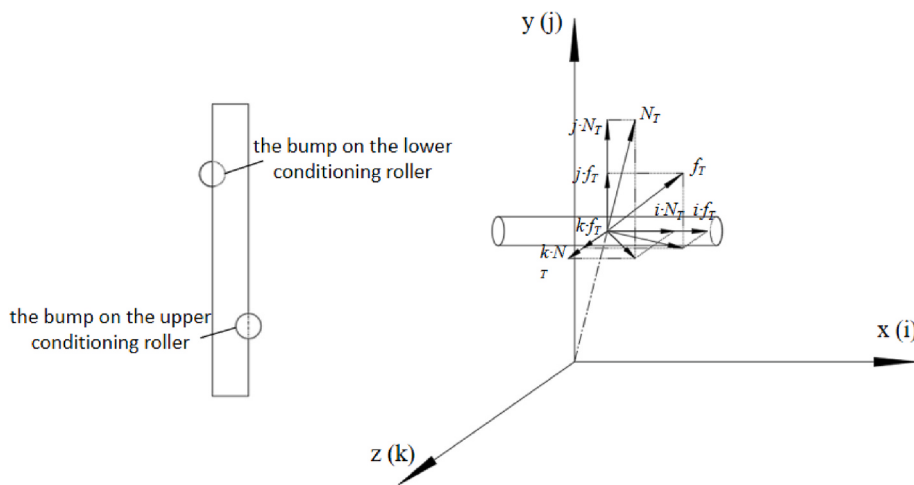


Fig. 9. The mechanical mechanism of bumps damage to alfalfa fibres.

By combining Eqs (15)–(18), the coordinates of each bump are obtained, as shown in Eq. (19).

$$\left\{ \begin{array}{l} a_1(x_1, y_1, z_1) = a_1(0, y_1, z_1) \\ a_2(x_2, y_2, z_2) = a_2\left(a, y_1 - R_1 + R_1 \cos\left(\arcsin \frac{a}{R_1}\right), z_1\right) \\ a_3(x_3, y_3, z_3) = a_3\left(\left(a + \sin \beta, y_1 - R_1 + R_1 \cos\left(\arcsin \frac{a}{R_1}\right), z_1 - a \cos \beta\right)\right. \\ \quad \left.a_4(x_4, y_4, z_4) = a_4(a \sin \beta, y_1, z_1 - a \cos \beta)\right. \\ b_5(x_5, y_5, z_5) = b_5\left(R_2 \sin\left(\frac{\pi}{3} + \arcsin \frac{a - a^3(1 - \sin \beta)^2}{R_1}\right), R_2 \cos\left(\frac{\pi}{3} + \arcsin \frac{a - a^3(1 - \sin \beta)^2}{R_1}\right), \right. \\ \quad \left.z_1 - a^2(1 - \sin \beta) \sin[\arccos(a - a \sin \beta)]\right) \\ a_n(x_n, y_n, z_n) = a_n\left(na, \frac{na}{\tan\left(\arcsin \frac{a}{R_1}\right)}, z_1\right) \end{array} \right. \quad (19)$$

Fig. 9 presents a transient mechanical analysis of alfalfa stems during the conditioning process. Adjacent bumps exert opposing force components along the positive y- and z-directions on the alfalfa stems, producing micro-rubbing action through the combined effects of compressive stress and frictional forces. Based on this force relationship, Eq. (20) is derived.

$$\left\{ \begin{array}{l} F_{Tx} = N_{T1} \cdot i_1 + f_{T1} \cdot i_1 + \dots + N_{Tm} \cdot i_m + f_{Tm} \cdot i_m \\ F_{Ty} = N_{T1} \cdot j_1 + f_{T1} \cdot j_1 + \dots + N_{Tm} \cdot j_m + f_{Tm} \cdot j_m \\ F_{Tz} = N_{T1} \cdot k_1 + f_{T1} \cdot k_1 + \dots + N_{Tm} \cdot k_m + f_{Tm} \cdot k_m \end{array} \right. \quad (20)$$

where F_{Tx} , F_{Ty} and F_{Tz} are the components of the force exerted by the bump on the alfalfa stem along the x-, y- and z-axes, respectively (N); i, j and k are the unit vectors in the positive directions of the x-, y- and z-axes; and N_{Tm} and f_{Tm} denote the normal force and frictional force exerted by the m -th bump on the stem, respectively (N).

2.4. Finite element simulation of alfalfa conditioning

2.4.1. Parameter calibration process

The FEM offers significant advantages in simulating the interaction between flexible crops and elastic or rigid mechanical components, effectively revealing the deformation and failure mechanisms of crops. This insight is crucial for the design and optimisation of mechanical components (Govilas et al., 2023; Huang et al., 2023; Niu et al., 2022; Stopa et al., 2019). Whether employing the FEM or the discrete element method, when certain material parameters cannot be directly measured due to factors such as geometric dimensions or material morphology, parameter calibration based on bulk material properties becomes

Table 1
Mechanical parameters of alfalfa.

Simulation Parameters	Value
Poisson's ratio in the isotropic plane	0.42
Poisson's ratio in the anisotropic plane	0.02
Radial elastic modulus (MPa)	28.66
Sliding friction coefficient between alfalfa stem and steel plate	0.60
Rolling friction coefficient between alfalfa stem and steel plate	0.15
Axial elastic modulus (MPa)	550.72
Axial shear modulus (MPa)	6.10
Radial shear modulus (MPa)	60.32

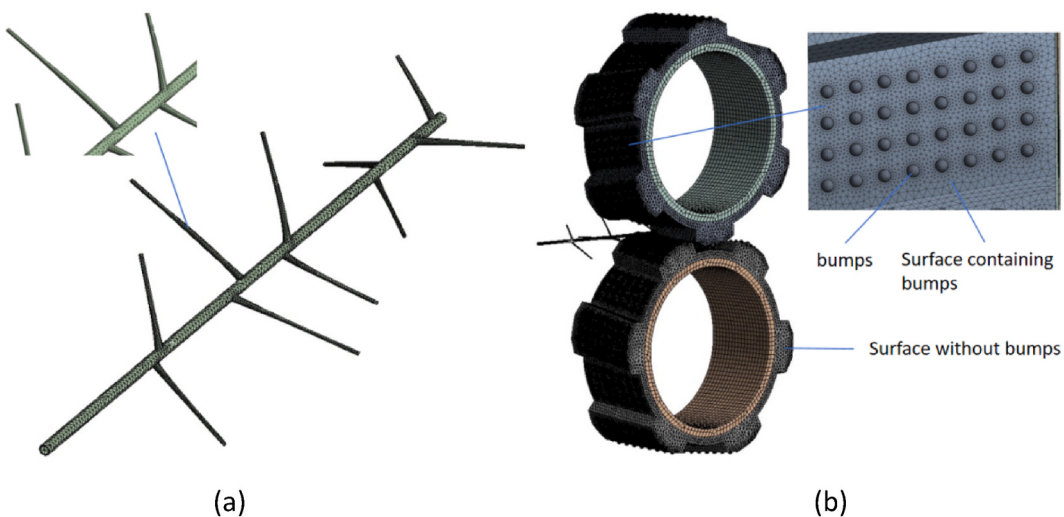


Fig. 10. Simulation modelling and mesh generation: (a) mesh generated on the stem and (b) mesh generated on the conditioning rollers.

Table 2
Factor level coding for the response surface test (simulation test).

Level	Factors		
	Bump diameter A (mm)	Non-interference distance B (mm)	helix angle C (°)
-1	2	0	10
0	3	1.5	25
1	4	3	40

necessary (Marigo & Stitt, 2015; Sun et al., 2024). By adjusting these material parameters, simulation results can be brought into closer alignment with experimental measurements. Given that multiple parameter combinations may yield similar simulation outcomes, specific validation experiments are essential to verify the calibration results. Owing to the difficulty of accurately measuring material parameters such as the radial elastic modulus and Poisson's ratio of thin-walled crop stems, we proposed a finite element parameter calibration method for the alfalfa conditioning model and validated the calibration results through experimental verification. The detailed results are presented in Jin et al. (2024). The FEM parameters of alfalfa are listed in Table 1.

2.4.2. Optimisation of bump structure parameters in simulation

Based on the model parameters obtained in Section 2.4.1, simulations of alfalfa conditioning were carried out. The profile material of the conditioning roller was TPU. The sliding and rolling friction coefficients between the alfalfa and the conditioning roller were determined via slope tests, measured as 0.75 and 0.13, respectively. When conducting simulations, both feasibility and efficiency must be considered; hence, the model was simplified to some extent. It was assumed that the

material parameters of alfalfa stems and lateral branches were identical, with differences in mechanical properties arising solely from their geometric shapes (Carvalho et al., 2016). Following the methods described by Carvalho et al. (2016) and Souza et al. (2018), the leaves were omitted, simplifying the alfalfa to stems and lateral branches, as shown in Fig. 10. The stem length was 170 mm. The mesh size was 1 mm for the alfalfa stem and 0.5 mm for the lateral branches. To prevent geometric distortion, local mesh refinement was applied to the bumps on the conditioning roller: the mesh size for the bumps was 0.6 mm, 2.5 mm for geometric surfaces containing bumps and 3.5 mm for surfaces without bumps.

Based on the mechanical mechanism of fibre disruption in alfalfa stems by bumps (Eq. (20)), a bump diameter larger than the alfalfa stem diameter may result in increased stem breakage and loss, whereas a bump diameter that is too small or a centre distance that is too large may fail to effectively break the stem fibres, thereby reducing the uniformity of disruption. According to Eq. (12), to ensure no interference occurs between bumps, the edge length a (also the centre distance) of the rhombus on the projection plane should be greater than a_{\min} . The 'non-interference distance' $B = a - a_{\min}$ was specified, and the centre distance adjusted by varying B . Based on statistical analysis of stem diameters, the bump diameter range was set between 2 and 4 mm, and the non-interference clearance distance between bumps ranged from 0 to 3 mm. Increasing the helix angle of the conditioning roller raises the number of bumps and material costs; therefore, the helix angle was restricted to a range of 10°–40° in accordance with design requirements. To investigate the effects of different structural parameters on alfalfa damage and the interactions between experimental factors, the Box-Behnken experimental design method was employed for response surface testing. Bump diameter A , non-interference distance B and helix angle C were used as experimental factors, while the number of broken branches and instances of non-fracture damage served as evaluation indicators. The factor levels are summarised in Table 2. The number of broken branches comprises the total of broken lateral branches and stem breaks, whereas non-fracture damage refers to damage shorter than the stem diameter.

2.5. Alfalfa conditioning experiment

The experimental site was located at the alfalfa planting base in Wuji County, Hebei Province, China. The alfalfa variety used was 'Zhongmu 5', known for its enhanced salt tolerance and suitability for cultivation in the Huang Huai Hai region of China. The alfalfa was harvested manually and was free from pests and diseases. The moisture content of

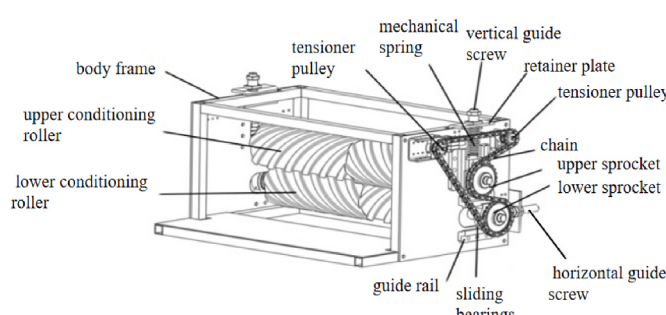


Fig. 11. Schematic diagram of the alfalfa conditioning experimental device.

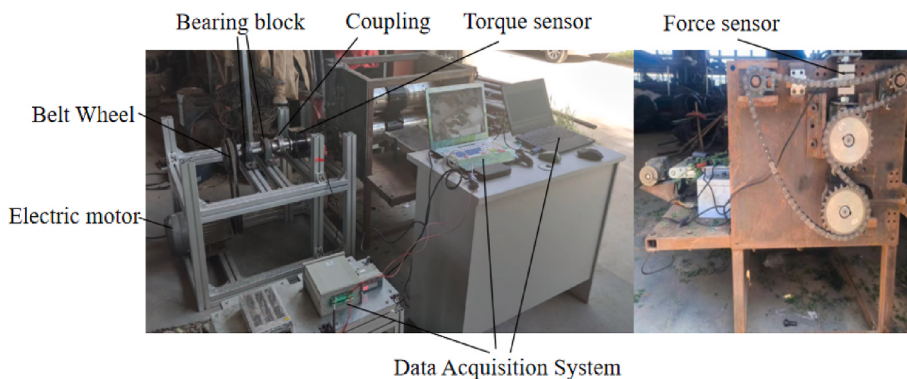


Fig. 12. Alfalfa conditioning test bench.

Table 3

Parameter levels used in model validation experiments.

Thickness(mm)	Speed (r min ⁻¹)	Speed (r min ⁻¹)	Thickness (mm)
10 ± 2	400	400	5 ± 2
	450		10 ± 2
	500		15 ± 2

Table 4

Factor level coding table for the response surface test (conditioning test).

Level	Factors		
	Roller gap D (mm)	Feed rate E (g s ⁻¹)	roller rotational speed F (r min ⁻¹)
-1	2	450	600
0	3	825	800
1	4	1200	1000

the alfalfa used in the experiment was consistently above 70 %.

A schematic diagram of the alfalfa conditioning test bench structure is presented in Fig. 11. The test bench comprised a conditioning mechanism, a gap and angle adjustment mechanism, and a transmission mechanism, with the alfalfa feed rate controlled by a conveyor belt. To verify the conditioning model, a force measurement system and a torque measurement system were each installed twice on the test bench, as shown in Fig. 12. One end of the force sensor (Bengbu High-Precision Sensor Co., Ltd., Bengbu, China; range 0–1000 kg, ±0.03 % FS) was fixed to the frame, while the other end was connected to a vertical sliding bearing via a screw. Based on mechanical principles, the load measured by the force sensor was approximately half of the total load exerted on the alfalfa. One end of the torque sensor (Bengbu High-Precision Sensor Co., Ltd., Bengbu, China; range 0–100 N m, 0.1 % FS) was connected to the shaft of the conditioning roller, with the other end connected to the motor. Both sensors were calibrated prior to the experiment following the manufacturer's calibration procedures. A zero-load output measurement was conducted for 30 min before testing to ensure that zero drift Z did not exceed 0.2 % FS.

Due to the broad applicability of the alfalfa conditioning model to rollers with any spiral tooth structure, experiments were conducted using traditional rectangular tooth conditioning rollers (RTCR) for ease of calculation during model validation. The conditioning roller was made of TPU, and the specimen length was 160 mm. By varying the alfalfa thickness and the conditioning roller speed, force and torque data were collected under different conditions. The conditioning energy was calculated using Eq. (21) and compared with the values obtained via Eq. (10) to validate the conditioning model. The calculation based on Eq. (10) was referred to as the force method, while the method based on Eq. (21) was termed the torque method. The experimental conditions are detailed in Table 3. The alfalfa thickness corresponded to the average

stem thickness when alfalfa formed uniform grass strips.

$$W_{TS} = \frac{W_1 - W_0}{m} = \frac{2\pi N \int_{t_0}^t (T(t) - T_0) dt}{60m} \quad (21)$$

where W_{TS} is the conditioning energy (J kg^{-1}); W_0 is the no-load energy of the test bench (J); W_1 is the total energy consumed during the conditioning process (J); T_0 is the no-load torque of the test bench (N m); $T(t)$ is the torque at time t (N m); and N is the roller rotational speed (r min^{-1}).

The conditioning energy error η_e is defined by Eq. (22).

$$\eta_e = \frac{|W_{FS} - W_{TS}|}{W_{TS}} \times 100\% \quad (22)$$

2.6. Optimisation of working parameters

According to the conditioning model (Eq. (10)), the main working parameters influencing the conditioning effect are feed rate, roller gap and roller rotational speed. To determine the optimal working parameters, a response surface test was conducted using conditioning rate, conditioning loss rate and conditioning energy as evaluation indicators. The factor levels are listed in Table 4. Preliminary experiments showed that when the roller speed exceeds 1000 r min^{-1} , the alfalfa loss rate significantly increases. Therefore, the roller rotational speed was set between 600 and 1000 r min^{-1} . Before the experiment, alfalfa was collected and weighed from five randomly selected 1 m × 1 m plots, yielding an average biomass of 1697.5 g m^{-2} . The mower conditioner has a cutting width of 1.2 m, a forward speed range of 1–2.5 m s^{-1} and a conditioning roller length of 730 mm. The corresponding feed rate for the mower conditioner was 2037–4243.75 g s^{-1} . Based on this, the feed rate for the 160-mm conditioning roller specimen was scaled to 446.60–1116.80 g s^{-1} and was controlled within 450 ± 30 to 1200 ± 30 g s^{-1} using a conveyor belt.

After the experiment, alfalfa plants longer than 7 cm with more than 50 % stem damage were selected and weighed. The conditioning rate was calculated using Eq. (23).

$$C_r = \frac{m_c}{m} \times 100\% \quad (23)$$

where m_c is the mass of alfalfa meeting the conditioning criteria (kg).

Alfalfa with lengths less than 7 cm was also selected and weighed. The conditioning loss rate was calculated using Eq. (24).

$$B_r = \frac{m_b}{m} \times 100\% \quad (24)$$

where m_b is the mass of alfalfa lost or broken into small pieces (kg).

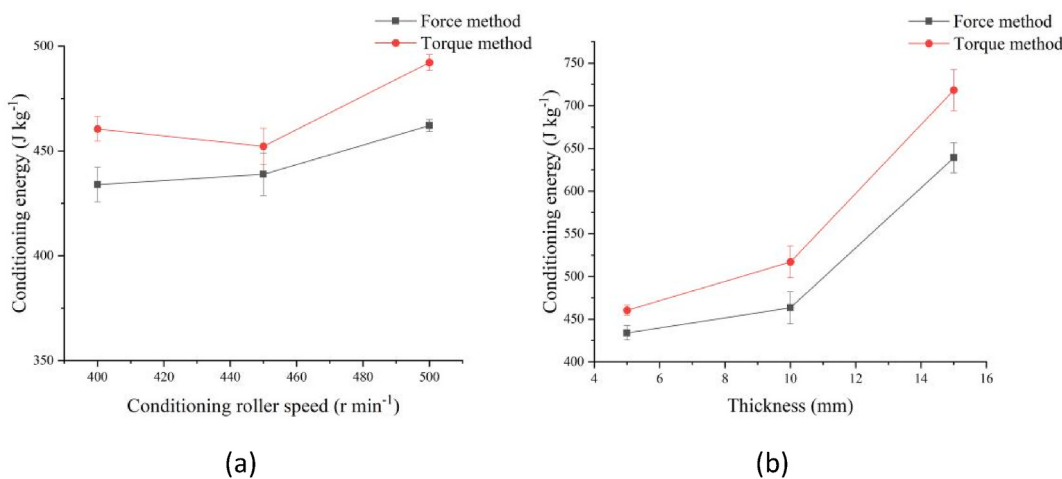


Fig. 13. Comparison of two methods for calculating conditioning energy: (a) conditioning energy at different speeds and (b) conditioning energy at varying alfalfa thicknesses.

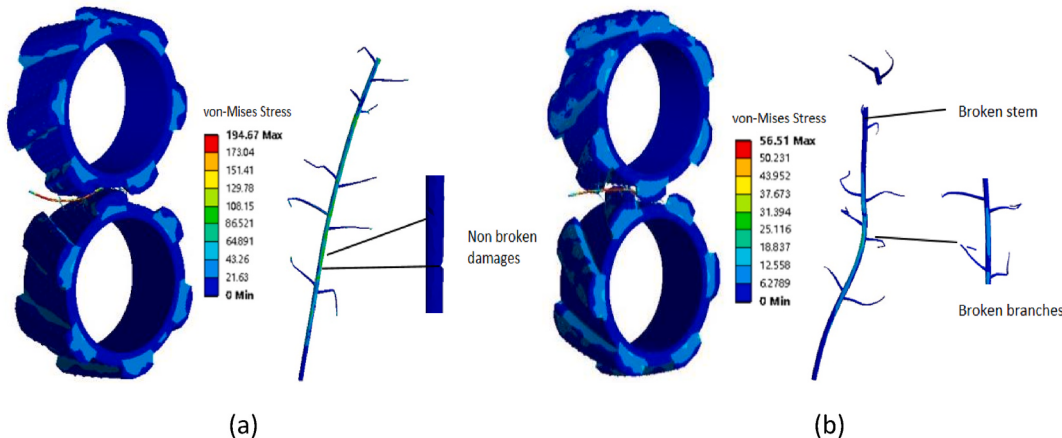


Fig. 14. Finite element simulation results of alfalfa conditioning: (a) non-fracture damage after conditioning and (b) broken stems and branches after conditioning.

Table 5

Results of the Box-Behnken experiment (simulation test).

Number	A	B	C	The average number of broken branches	The average number of non-fracture damage occurrences
1	1	0	1	4.67	2.67
2	0	0	0	1.67	7.33
3	1	0	-1	6.33	3.67
4	0	0	0	2.33	7.67
5	-1	0	-1	0.67	1.33
6	1	1	0	7.67	5.33
7	0	0	0	1.67	7.67
8	-1	0	1	1.00	2.33
9	0	0	0	2.00	8.67
10	-1	-1	0	0.33	0.67
11	0	0	0	1.67	8.33
12	0	-1	-1	1.00	3.67
13	0	1	1	2.67	5.67
14	-1	1	0	1.00	1.67
15	0	-1	1	3.00	6.34
16	0	1	-1	4.33	7.67
17	1	-1	0	3.33	3

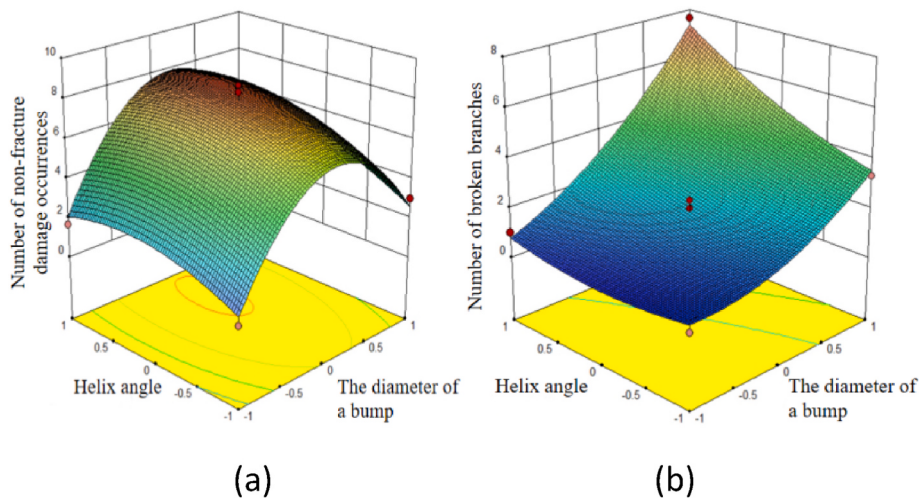
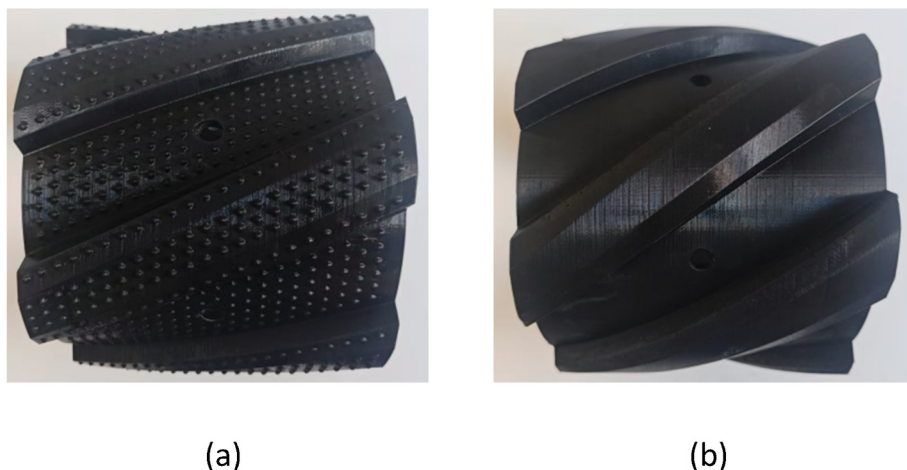
2.7. Alfalfa drying experiment

The experiment was conducted in late April during the first harvest of alfalfa hay in Hebei Province. Environmental conditions were $26.5^{\circ}\text{C} \pm 1^{\circ}\text{C}$ temperature and 42 % relative humidity under clear and windless weather, with a measured ground temperature of 29.3°C during testing. Following the method described in Section 2.6, the optimal operating parameters for the HTCR (without bumps) were determined as 750 r min^{-1} rotational speed, 712 g s^{-1} feed rate and a roller gap of 2.03 mm. For the RTCR, the optimal parameters were 703 r min^{-1} , 695 g s^{-1} and 3.02 mm, respectively. Conditioning tests were performed using three types of conditioning rollers. The alfalfa conditioned first was immediately placed in fresh-keeping bags for storage. After the conditioning test, samples were collected from alfalfa treated by the three rollers and untreated alfalfa (control group). Three replicates were taken under each condition, each containing $400 \pm 50 \text{ g}$ of alfalfa for natural drying. Weighing was conducted every 60 min over a 240-min drying period. After the drying test, the samples were collected and placed in a drying oven, dried at 104°C for 24 h, and the mass of the specimens was measured. The moisture content of alfalfa was calculated using Eq. (25).

Table 6

Analysis of variance of experimental results (simulation test).

Source	Number of broken branches					Number of non-fracture damage occurrences				
	Sum of Square	df	F	p	Significance	Sum of Square	df	F	p	Significance
Model	65.89	9	42.12	<0.0001	**	114.40	9	33.85	<0.0001	**
A	45.12	1	259.65	<0.0001	**	9.40	1	25.02	0.0016	**
B	8.02	1	46.15	0.0003	**	5.54	1	14.77	0.0064	**
C	0.12	1	0.70	0.4289		0.056	1	0.15	0.7106	
AB	3.37	1	19.37	0.0032	**	0.44	1	1.18	0.3138	
AC	0.99	1	5.70	0.0484	*	1.00	1	2.66	0.1467	
BC	3.35	1	19.27	0.0032	**	5.45	1	14.52	0.0066	
A^2	2.80	1	16.13	0.0051	**	77.93	1	207.54	<0.0001	**
B^2	0.67	1	3.85	0.0906	*	3.92	1	10.43	0.0145	*
C^2	0.98	1	5.66	0.0489	*	5.40	1	14.37	0.0068	**
Residual	1.22	7				2.63	7			
Lack of fit	0.87	3	3.32	0.1383		1.43	3	1.58	0.3262	
Pure Error	0.35	4				1.20	4			
Cor. Total	67.10	16				117.03	16			

Note: * represents a significant value ($p < 0.05$), and ** represents a highly significant value ($p < 0.01$).**Fig. 15.** Influence of experimental factors on the number of non-fracture damage occurrences and broken branches: (a) interaction between helix angle and bump diameter on non-fracture damage occurrences, (b) interaction between helix angle and bump diameter on broken branches.**Fig. 16.** Conditioning rollers produced by 3D printing: (a) HTCR (with bumps) and (b) HTCR (without bumps).

$$W_f = \frac{m_f - m_d}{m_f} \times 100\% \quad (25)$$

where W_f is the Moisture content of alfalfa (%); m_f is the fresh mass of alfalfa (kg); m_f is the mass of alfalfa at time t during drying (kg); and m_d is the dry mass of alfalfa after oven drying (kg).

3. Results

3.1. Model validation

Fig. 13 presents the conditioning energy results using two methods: the torque method and the force method. When the alfalfa thickness was 5 mm, increasing the roller rotational speed resulted in average conditioning energies of 460.52 J kg⁻¹, 452.30 J kg⁻¹ and 492.27 J kg⁻¹, using the torque method, and 434.01 J kg⁻¹, 438.91 J kg⁻¹ and 462.19 J kg⁻¹ using the force method, respectively. The maximum difference between the two methods was 30.08 J kg⁻¹, while the minimum difference was 13.39 J kg⁻¹. At a constant speed of 400 r min⁻¹, as alfalfa thickness increased, the average conditioning energies calculated by the torque method were 460.52 J kg⁻¹, 517.06 J kg⁻¹ and 718.29 J kg⁻¹, compared to 434.01 J kg⁻¹, 463.43 J kg⁻¹ and 639.17 J kg⁻¹ by the force method. The maximum difference between methods was 79.12 J kg⁻¹, corresponding to an 11.0 % conditioning energy error, while the minimum difference was 26.51 J kg⁻¹, with a 5.8 % error.

3.2. Simulation results

The simulation results are presented in **Fig. 14**. Among the three factors studied, the bump diameter had the most significant effect on the von Mises stress experienced by the alfalfa stem during conditioning. Using a centre distance of 1.5 and a helix angle of 25° as an example, when the bump diameter increased from 2 mm to 4 mm, the von Mises stress initially rose sharply and then decreased. Specifically, at bump diameters of 2, 3 and 4 mm, the von Mises stresses were 24.25 ± 1.27 MPa, 195.01 ± 1.94 MPa and 56.01 ± 4.23 MPa, respectively.

The Box–Behnken experimental design table was generated using Design-Expert 13 software, and the corresponding simulation results are presented in **Table 5**.

Regression analysis of the experimental data yielded the regression models for the average number of broken branches (N_b) and the average number of non-fracture damage occurrences (N_c), expressed as Eq. (26).

$$\begin{cases} N_b = 2.38A + 1.00B - 0.12C + 0.92AB - 0.50AC - 0.91BC + 0.82A^2 \\ \quad + 0.40B^2 + 0.48C^2 + 1.87 \\ N_c = 1.08A + 0.83B + 0.08C + 0.33AB - 0.50AC - 1.17BC - 4.30A^2 \\ \quad - 0.96B^2 - 1.13C^2 + 7.93 \end{cases} \quad (26)$$

The variance analysis of the experimental results is presented in **Table 6**. The significance levels of the quadratic regression models for both the number of broken branches and the number of non-fracture damage occurrences were $p \leq 0.01$, indicating that the models are statistically significant. The p -values for the lack of fit tests of both models were greater than 0.05, confirming a good fit between the models and the experimental data. For the number of broken branches, the order of factor influence was $A > B > AB > BC > AC > C$. For the radial contact force, the factors ranked as $A > B > BC > AC > AB > C$. The experimental results are illustrated in **Fig. 15**.

Based on the simulation text results, the goal is to minimise the number of broken branches and maximise the number of non-fracture damages. The objective function and constraints are given in Eq. (27).

$$\begin{cases} \min N_b(A, B, C) \\ \max N_c(A, B, C) \\ 2 \text{ mm} \leq A \leq 4 \text{ mm} \\ 0 \text{ mm} \leq B \leq 3 \text{ mm} \\ 10^\circ \leq C \leq 40^\circ \end{cases} \quad (27)$$

The optimal parameter combination obtained using Design-Expert 13 software was a bump diameter of 2.85 mm, a helix angle of 23.85° and a non-interference distance of 1.61 mm. Under these optimal parameters, the number of broken branches was 0.67, and the number of non-fracture damage occurrences was 7.67.

3.3. Optimisation results of working parameters

According to the simulation results in Section 3.2, a conditioning roller profile with a length of 160 mm was produced using 3D printing technology, as shown in **Fig. 16**.

The test results are presented in **Table 7**. Regression analysis was conducted on the experimental data to obtain the regression model, Eq. (28), for conditioning rate, conditioning loss rate and conditioning energy.

$$\begin{cases} C_r = -1.99D - 0.45E + 0.17N + 0.22DE + 0.72DN + 1.24EF - 3.44D^2 \\ \quad - 0.97E^2 - 0.23N^2 + 96.66 \\ B_r = -0.95D - 0.47E + 0.57N - 0.31DE - 0.21DN - 0.23EN + 0.65D^2 \\ \quad + 0.70E^2 + 0.29N^2 + 2.33 \\ W_{TS} = -130.88D + 27.44E + 37.92N + 21.45DE + 12.36DN + 26.90EN \\ \quad + 122.50D^2 + 23.67E^2 + 34.98N^2 + 630.34 \end{cases} \quad (28)$$

The variance analysis of the experimental results is presented in **Table 8**. The p -values of the quadratic regression models for conditioning rate, conditioning loss rate and conditioning energy were all less than 0.01, indicating the statistical significance of the surface regression models. The p -values for lack of fit for all models were greater than 0.05, demonstrating good model fit. The interaction term DN represents the interaction between roller gap and roller rotational speed. The roller gap determines the compression intensity applied to the stems, while the roller rotational speed affects the time the material spends passing through the conditioning zone. When the roller gap is large, an excessively high roller rotational speed shortens the stem compression time, which may result in insufficient conditioning (i.e. a decrease in conditioning rate). The interaction term EN represents the interaction between feed rate and roller rotational speed. The feed rate determines the total mass of material processed per unit time. A high feed rate requires a correspondingly high roller rotational speed to maintain conditioning efficiency. However, if the roller rotational speed is too high, material slippage may occur, reducing the conditioning rate. The interaction

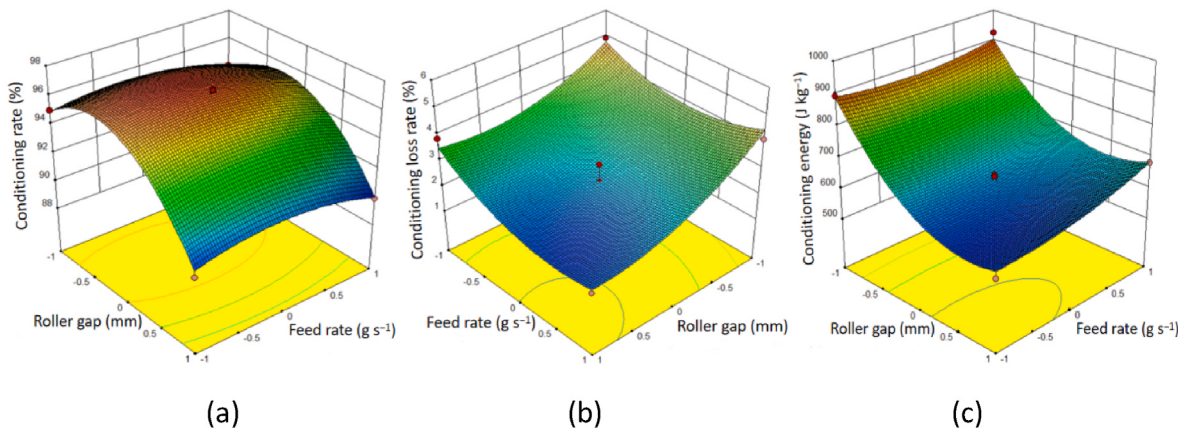
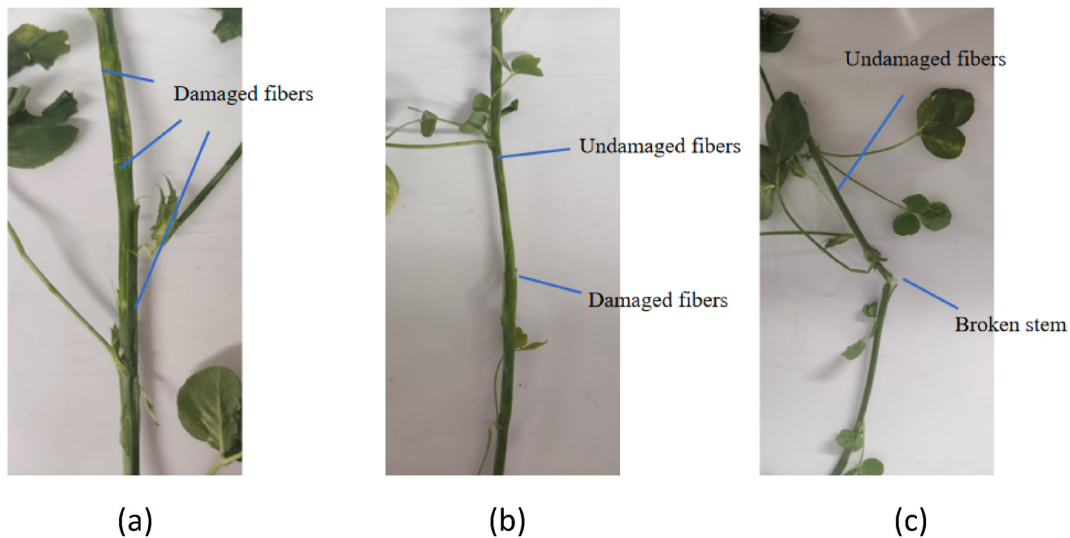
Table 7
Results of the Box–Behnken experiment (conditioning test).

Number	D	E	N	Conditioning rate (%)	Conditioning loss rate (%)	Conditioning energy (J kg ⁻¹)
1	-1	0	1	94.2	5.3	932.13
2	-1	-1	0	95.0	4.9	893.92
3	0	0	0	96.7	1.9	634.15
4	0	1	1	96.2	3.2	761.67
5	0	1	-1	93.5	3.2	652.01
6	0	0	0	96.0	2.1	621.50
7	-1	1	0	94.0	4.1	925.12
8	0	-1	-1	97.2	3.0	670.13
9	1	0	1	92.3	2.8	719.34
10	0	0	0	96.9	2.3	615.09
11	1	0	-1	90.3	1.6	598.80
12	0	0	0	96.8	2.4	637.33
13	-1	0	-1	95.1	3.3	861.02
14	0	0	0	96.9	3.0	643.65
15	1	1	0	89.9	1.8	682.01
16	1	-1	0	90.0	3.9	565.01
17	0	-1	1	94.9	4.1	672.19

Table 8

Analysis of variance of the experimental results (conditioning test).

Source	Conditioning rate (%)		Conditioning loss rate (%)		Conditioning energy consumption (J kg^{-1})	
	Sum of Square	P	Sum of Square	P	Sum of Square	P
Model	98.23	<0.001**	16.94	0.0062**	2.246 E+005	<0.001**
D	31.60	<0.001**	7.18	0.0009**	1.370 E+005	<0.001**
E	1.60	0.0288*	1.78	0.0292*	6025.82	0.0088**
N	0.22	0.3455	2.63	0.0126*	11504.17	0.0016**
DE	0.19	0.3721	0.37	0.2512	1840.41	0.0873
DN	2.04	0.0173*	0.17	0.4283	610.83	0.2900
EF	6.15	0.0010*	0.21	0.3819	2894.44	0.0415*
D^2	49.81	<0.0001**	1.75	0.0300*	53286.39	<0.0001**
E^2	4.00	0.0034*	2.08	0.0212*	2359.87	0.0592
N^2	0.23	0.3317	0.35	0.2653	5152.52	0.0127*
Residual	1.49		1.67		3264.26	
Lack of fit	0.96	0.2042	0.96	0.2846	2713.02	0.0504
Pure Error	0.53		0.71		551.24	
Cor. Total	99.72		18.61		2.278 E+005	

Note: * represents a significant value ($p < 0.05$), and ** represents a highly significant value ($p < 0.01$).**Fig. 17.** Influence of experimental factors on conditioning rate, conditioning loss rate and conditioning energy at a roller speed of 800 r min^{-1} : (a) interaction between roller gap and feed rate on the conditioning rate, (b) interaction between roller gap and feed rate on the conditioning loss rate and (c) interaction between roller gap and feed rate on the conditioning energy.**Fig. 18.** Damage to alfalfa stems after conditioning: (a) conditioned using HTCR (with bumps), (b) conditioned using HTCR (without bumps) and (c) conditioned using RTCH.

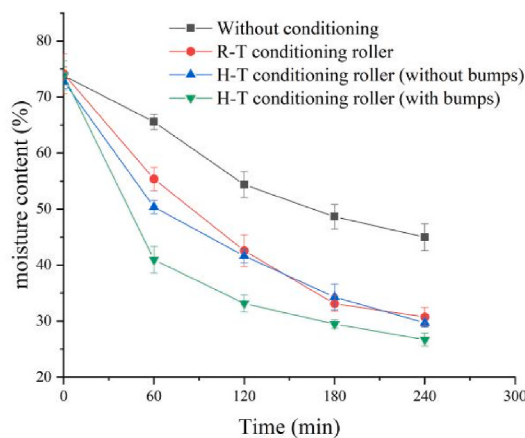


Fig. 19. Changes in the moisture content of alfalfa over time.

term's *p*-value <0.05 indicates that this interaction has a statistically significant impact on the experimental factors. These results imply that simply adjusting a single parameter cannot achieve optimal performance; instead, a coordinated adjustment of parameter combinations is required to balance the conditioning rate, conditioning loss rate and conditioning energy consumption. The order of factors affecting the conditioning rate was $D > EN > DN > E > N > DE$. The order of factors affecting the conditioning loss rate was $D > N > E > DE > EN > DN$. The order of factors affecting the conditioning energy was $D > N > E > EN > DE > DN$. The experimental results are illustrated in Fig. 17.

Based on the Box-Behnken test results, the goals are to maximise the conditioning rate, minimise the conditioning loss rate and minimise the conditioning energy. The objective function and constraints are given in Eq. (29).

$$\left\{ \begin{array}{l} \max C_r(D, E, N) \\ \min B_r(D, E, N) \\ \min W_{Ts}(D, E, N) \\ 2 \text{ g/s} \leq D \leq 4 \text{ g/s} \\ 600 \text{ rpm} \leq E \leq 1000 \text{ rpm} \\ 2 \text{ mm} \leq N \leq 4 \text{ mm} \end{array} \right. \quad (29)$$

The optimal parameter combination was obtained using Design-Expert 13 software: a feed rate of 779 g s^{-1} , roller rotational speed of 683 r min^{-1} , and roller gap of 3.13 mm. Under these conditions, the conditioning rate, conditioning loss rate and conditioning energy were 96.9 %, 2.0 % and 652.04 J kg^{-1} , respectively.

3.4. Results of drying experiment

Fig. 18 shows the damage to alfalfa stems after conditioning. The alfalfa stems conditioned using HTCR (with bumps) exhibited the most significant damage, with an average damage rate of 82.3 %. The average damage rate for stems conditioned using HTCR (without bumps) was 60.4 %, while the average damage rate after RTCH conditioning was 53.8 %.

The drying results of alfalfa are shown in Fig. 19. Within the first 60 min, the moisture content of alfalfa after HTCR (with bumps) conditioning decreased from 73.9 % to 41.0 %, representing the largest reduction of 32.9 % among the four conditions. The moisture content of alfalfa after HTCR (with bumps) and RTCH conditioning decreased by 22.4 % and 18.6 %, respectively. Unconditioned alfalfa showed the smallest decrease, with a reduction of 8.3 % during the same period. Between 60 and 120 min, the rate of moisture loss in conditioned alfalfa slowed slightly. The moisture content decreased by 7.8 %, 7.3 % and 9.4 % after HTCR (with bumps), HTCR (without bumps) and RTCH conditioning, respectively. Interestingly, the moisture content of unconditioned alfalfa slightly increased, with an overall reduction of 11.2 %.

During the 120–240 min period, moisture content continued to decline. The reductions observed were 6.4 %, 11.9 % and 11.8 % for (with bumps), HTCR (without bumps) and RTCH conditioning, respectively. The moisture content of unconditioned alfalfa decreased by 9.4 %. Overall, HTCR (with bumps) more effectively disrupts the fibre structure of alfalfa stems, accelerating water evaporation. Compared to HTCR (without bumps) and RTCH, alfalfa conditioned with HTCR (with bumps) demonstrated superior performance during both the initial moisture reduction below 40 % and the subsequent reduction below 30 %.

4. Discussion

In this study, an alfalfa conditioning model based on the energy method was established, and the main structural and operational parameters affecting the alfalfa conditioning effect were identified. Compared with the findings of Song et al. (2021), the two methods produced similar results. The conditioning energy calculated using the force method was slightly lower than that calculated using the torque method. This discrepancy may be attributed to several factors. First, the model simplified alfalfa as a uniform material. In reality, however, alfalfa is heterogeneous due to variations in stem shape, leaves and lateral branches. Second, although the hardness of the conditioning profile exceeded that of the alfalfa stem, some deformation still occurred during conditioning, resulting in the storage of elastic potential energy. Third, the torque method includes additional energy generated during conditioning caused by vibrations from alfalfa feeding, which is not accounted for in the force method.

To improve the uniformity of alfalfa disruption, we developed a bump-type conditioning roller and optimised its structural parameters using the FEM. However, several challenges requiring further investigation to enhance conditioning effectiveness were identified during the experimental process. The analysis indicates that the bump-type conditioning roller demonstrates satisfactory alfalfa conditioning performance and offers two distinct advantages over conventional rollers. First, the incorporation of bumps increases the actual contact area between the alfalfa and the roller, thereby enhancing the utilisation efficiency of the conditioning zone. Second, adjacent bumps apply gentle rubbing actions to the stems, improving both the intensity and uniformity of surface fibre disruption. Compared with previous studies (Greenlees et al., 2000; Jin et al., 2024; Song et al., 2021), although the bump-type conditioning roller did not significantly improve the conditioning rate (both exceeding 95 %), it substantially increased the stem damage rate after conditioning (from 53.8 % to 82.3 %) and demonstrated a shorter drying time in drying trials. Nonetheless, the bump structure still holds potential for further optimisation. For example, compared with the findings of Qiao et al. (2024), the conditioning loss rate slightly increased, which may be attributed to both the inherent variability of alfalfa and the more severe damage induced by the bump structure. Future studies should focus on developing flexible adjustment technologies for roller gaps to mitigate the loss rate. Additionally, as the profile materials undergo continuous wear, research is needed on the impact of material degradation on conditioning effectiveness to determine the service life of the conditioning roller. Finally, there remains a discrepancy between the drying conditions in this experiment and those in actual field conditions. Subsequent efforts should prioritise large-scale field harvesting trials to further validate the operational effectiveness of the conditioning roller.

5. Conclusions

To clarify the main factors affecting the conditioning effect of alfalfa, an alfalfa conditioning model was established. To enhance stem damage during conditioning, a conditioning roller with bumps was designed, and its structural and operational parameters were optimised. The main conclusions are as follows.

- (1) An alfalfa conditioning model was established based on the force and geometric relationship between alfalfa and rollers. The accuracy of the model was verified through conditioning experiments. The main factors affecting the conditioning effect of alfalfa included the frictional force between alfalfa and conditioning rollers, conditioning roller gap, alfalfa feed rate, conditioning roller helix angle, roller rotational speed, number and shape of roller teeth.
- (2) A conditioning roller with bumps capable of effectively disrupting stem fibres was designed. Finite element simulations of alfalfa conditioning were conducted, and optimal parameter combinations for bump diameter, bump non-interference distance and conditioning roller helix angle were determined through Box-Behnken experiments as 2.85 mm, 1.61 mm and 23.85°, respectively. Under these optimal parameters, the number of broken branches was 0.67, and the number of non-fracture damage occurrences was 7.67.
- (3) RSM experiments were carried out using conditioning rate, conditioning loss rate and conditioning energy as objective functions, with roller gap, roller rotational speed and feed rate as influencing factors. The optimal parameters were a roller gap of 3.13 mm, roller rotational speed of 683 r min⁻¹ and feed rate of 779 g s⁻¹. Conditioning experiments under these conditions resulted in a conditioning rate of 96.9 %, conditioning loss rate of 2.0 % and conditioning energy of 652.04 J kg⁻¹.
- (4) Drying experiments were conducted on 400 ± 50 g of alfalfa after conditioning under natural conditions. The drying results for alfalfa conditioned with HTCR (with bumps), HTCR (without bumps), RTCR and unconditioned alfalfa were compared. After HTCR (with bumps) conditioning, the moisture content decreased to around 40 % within 0–60 min. In contrast, HTCR (without bumps) and RTCR conditioning reduced moisture content below 40 % after 120 min. After 240 min, alfalfa conditioned with HTCR (with bumps) reached approximately 20 % moisture content, demonstrating a superior drying effect.

CRediT authorship contribution statement

Qiao Jin: Writing – review & editing, Writing – original draft, Data curation, Conceptualization. **Hongqian Li:** Validation. **Decheng Wang:** Writing – review & editing, Project administration, Funding acquisition. **Yong You:** Writing – review & editing, Funding acquisition. **Yunting Hui:** Writing – review & editing, Validation. **Sibiao Li:** Writing – review & editing.

Data availability statement

Data are available upon request, with the exception of those limited by privacy and ethical restrictions.

Statement on the use of generative AI and AI assisted technologies in the writing process

No generative AI or AI-assisted technologies were used during the preparation of this work.

Funding

This research were supported by the Major Scientific and Technological Innovation Project of Shandong Province (grant No. 2022CXGC020704-01) and the earmarked fund for CARS (CARS-34).

Declaration of competing interest

The authors declare that they have no known competing financial interests or personal relationships that could have appeared to influence

the work reported in this paper.

Acknowledgements

Qiao Jin: Writing – original draft, Visualisation, Investigation, Conceptualisation. Hongqian Li: Writing – review & editing. Decheng Wang: Writing – review & editing. Yong You: review & editing, Supervision, Project administration, Funding acquisition, Conceptualisation. Yunting Hui: Writing – review & editing. Sibiao Li: Writing – review & editing.

References

- Bacenetti, J., Lovarelli, D., Tedesco, D., Pretolani, R., & Ferrante, V. (2018). Environmental impact assessment of alfalfa (*Medicago sativa L.*) hay production. *The Science of the Total Environment*, 635, 551–558. <https://doi.org/10.1016/j.scitotenv.2018.04.161>
- Carvalho, E. d. A., Magalhães, R. R., & Santos, F. L. (2016). Geometric modelling of a coffee plant for displacements prediction. *Computers and Electronics in Agriculture*, 123, 57–63. <https://doi.org/10.1016/j.compag.2016.02.008>
- Chowdhury, M. R., Wilkinson, R. G., & Sinclair, L. A. (2023). Feeding lower-protein diets based on red clover and grass or alfalfa and corn silage does not affect milk production but improves nitrogen use efficiency in dairy cows. *Journal of Dairy Science*, 106(3), 1773–1789. <https://doi.org/10.3168/jds.2022-22607>
- Fychan, A., Leemans, D., Scott, M., Theobald, V., Sanderson, R., & Marley, C. (2016). Effect of mower-conditioner type during legume or grass harvesting on silage quality. *The Multiple Roles of Grassland in the European Bioeconomy: Proceedings of the 26th General Meeting of the European Grassland Federation*, 176–178. <https://www.cabidigitallibrary.org/doi/pdf/10.5555/20173038296>
- Galyon, H., Corl, B. A., & Ferreira, G. (2024). Ruminal passage rate and digestibility of fibre from dairy cows consuming diets containing alfalfa and orchardgrass hays with different concentrations of undegradable neutral detergent fibre. *Journal of Dairy Science*, 107(12), 10751–10760. <https://doi.org/10.3168/jds.2024-25264>
- Govilas, J., Clévy, C., Beaugrand, J., & Placet, V. (2023). Investigating the influence of plant fibre geometry on apparent transverse elastic properties through finite element analysis. *Composites Part A: Applied Science and Manufacturing*, 175, Article 107789. <https://doi.org/10.1016/j.compositesa.2023.107789>
- Greenlees, W. J., Hanna, H. M., Shinnars, K. J., Marley, S. J., & Bailey, T. B. (2000). A comparison of four mower conditioners on drying rate and leaf loss in alfalfa and grass. *Applied Engineering in Agriculture*, 16(1), 1. <https://doi.org/10.13031/2013.4984>
- Hualing, X., Yanping, Y., Yu, D., & Tai, W. (2021). Analysis on international development trends of alfalfa. *Chinese Bulletin of Botany*, 56(6), 740–750. <https://www.chinabullbotany.com/EN/10.11983/CBB21121>.
- Huang, J., Tian, K., Ji, A., Zhang, B., Shen, C., & Liu, H. (2023). Research on the construction of a finite element model and parameter calibration for industrial hemp stalks. *Agronomy*, 13(7). <https://doi.org/10.3390/agronomy13071918>
- Iannucci, A., Di Fonzo, N., & Martinelli, P. (2002). Alfalfa (*Medicago sativa L.*) seed yield and quality under different forage management systems and irrigation treatments in a mediterranean environment. *Field Crops Research*, 78(1), 65–74. [https://doi.org/10.1016/S0378-4290\(02\)00094-1](https://doi.org/10.1016/S0378-4290(02)00094-1)
- J Shinnars, K., M Wuest, J., E Cudoc, J., & E Herzmann, M. (2006). Intensive conditioning of alfalfa: Drying rate and leaf loss. *ASAE Annual Meeting*. <https://doi.org/10.13031/2013.22145>. Paper NO.061051.
- Jin, Q., You, Y., Wang, H., Ma, X., Wang, L., Wang, D., & Fang, X. (2024). Calibration and experimental verification of finite element parameters for alfalfa conditioning model. *Agriculture*, 14(10). <https://doi.org/10.3390/agriculture14101724>
- Kulkarni, K. P., Tayade, R., Asekova, S., Song, J. T., Shannon, J. G., & Lee, J. D. (2018). Harnessing the potential of forage legumes, alfalfa, soybean, and cowpea for sustainable agriculture and global food security. *Frontiers of Plant Science*, 9, 1314. <https://doi.org/10.3389/fpls.2018.01314>
- Marigo, M., & Stitt, E. H. (2015). Discrete element method (DEM) for industrial applications: comments on calibration and validation for the modelling of cylindrical pellets. *KONA Powder and Particle Journal*, 32, 236–252. <https://doi.org/10.14356/kona.2015016>
- Neres, M. A., Castagnara, D. D., Mesquita, E. E., Zambom, M. A., de Souza, L. C., Raballo de Oliveira, P. S., & Jobim, C. C. (2010). Production of alfalfa hay under different drying methods. *Revista Brasileira De Zootecnia-brazilian Journal of Animal Science*, 39 (8), 1676–1683. <https://doi.org/10.1590/S1516-35982010000800008>
- Niu, Z., Xu, Z., Deng, J., Zhang, J., Pan, S., & Mu, H. (2022). Optimal vibration parameters for olive harvesting from finite element analysis and vibration tests. *Biosystems Engineering*, 215, 228–238. <https://doi.org/10.1016/j.biosystemseng.2022.01.002>
- Palmonari, A., Fustini, M., Canestrari, G., Grilli, E., & Formigoni, A. (2014). Influence of maturity on alfalfa hay nutritional fractions and indigestible fibre content. *Journal of Dairy Science*, 97(12), 7729–7734. <https://doi.org/10.3168/jds.2014-8123>
- Qiao, J., Yong, Y., Decheng, W., Haiyi, W., Pengzhan, H., & Xianfa, F. (2024). Design and experiment of conditioning roller for alfalfa mower conditioner based on hexagonal irregular teeth. *Transactions of the Chinese Society for Agricultural Machinery*, 55(12), 239–248. <https://nyjxb.net/index.php/journal/article/view/2033>
- Rade, S., Aleksandar, V., Sasa, B., Rade, R., Dagoslav, D., & Dragan, P. V. (2019). Influence of harvesting on quality of alfalfa forage used for haylage and hay. *Journal*

- of Agricultural Sciences-tarım Bilimleri Dergisi, 25(3), 384–390. <https://doi.org/10.15832/ankutbd.434398>
- Razzaghi, A., Leskinen, H., Ahvenjärvi, S., Aro, H., & Bayat, A. (2022). Energy utilisation and milk fat responses to rapeseed oil when fed to lactating dairy cows receiving different dietary forage to concentrate ratio. *Animal Feed Science and Technology*, 293, Article 115454. <https://doi.org/10.1016/j.anifeedsci.2022.115454>
- Song, Z., Xing, S., Wang, Z., Tian, F., Wang, F., & Li, F. (2021). Design and experiment of measurement and control system for alfalfa conditioning test bench. *Transactions of the Chinese Society for Agricultural Machinery*, 52(2), 122–134 (in Chinese with English abstract) <https://link.cnki.net/urlid/11.1964.S.20201221.1636.032>.
- Souza, V. H. S., Dias, G. L., Santos, A. A. R., Costa, A. L. G., Santos, F. L., & Magalhães, R. R. (2018). Evaluation of the interaction between a harvester rod and a coffee branch based on finite element analysis. *Computers and Electronics in Agriculture*, 150, 476–483. <https://doi.org/10.1016/j.compag.2018.05.020>
- Stopa, R., Komarnicki, P., Kuta, Ł., Szyjewicz, D., & Ślupska, M. (2019). Modelling with the finite element method the influence of shaped elements of loading components on the surface pressure distribution of carrot roots. *Computers and Electronics in Agriculture*, 167, Article 105046. <https://doi.org/10.1016/j.compag.2019.105046>
- Sun, W., Sun, Y., Wang, Y., & He, H. (2024). Calibration and experimental verification of discrete element parametres for modelling feed pelleting. *Biosystems Engineering*, 237, 182–195. <https://doi.org/10.1016/j.biosystemseng.2023.12.006>
- Suwarno, S., Wittenberg, K. M., & McCaughey, W. P. (1999). Comparative characteristics during wilting for alfalfa conditioned by maceration or by a conventional roller-conditioner. *Canadian Journal of Animal Science*, 79, 509–517. <https://doi.org/10.4141/A99-018>
- Suwignyo, B., Aristia Rini, E., & Helmiyati, S. (2023). The profile of tropical alfalfa in Indonesia: A review. *Saudi Journal of Biological Sciences*, 30(1), Article 103504. <https://doi.org/10.016/j.sjbs.2022.103504>.
- Wang, D., He, C., Wu, H., You, Y., & Wang, G. (2017). Review of alfalfa full-mechanized production technology (Vol. 48, pp. 1–25). *Transactions of the Chinese Society for Agricultural Machinery*. <https://doi.org/10.6041/j.issn.1000-1298.2017.08.001> (in Chinese with English abstract).
- Wang, Q., & Zou, Y. (2020). China's alfalfa market and imports: Development, trends, and potential impacts of the U.S.–China trade dispute and retaliations. *Journal of Integrative Agriculture*, 19(4), 1149–1158. [https://doi.org/10.1016/S2095-3119\(19\)62832-7](https://doi.org/10.1016/S2095-3119(19)62832-7)
- Zhang, X., Liu, Y., Kong, F., Wang, W., & Li, S. (2023). Comparison of nutritional components, ruminal degradation characteristics and feed value from different cultivars of alfalfa hay. *Animals*, 13(4). <https://doi.org/10.3390/ani13040734>